

1 **Mid-Holocene Northern Hemisphere warming driven by Arctic**
2 **amplification and sea ice loss**

3 Hyo-Seok Park^{1*}, Seong-Joong Kim², Andrew L. Stewart³, Seok-Woo Son⁴ and Kyong-Hwan
4 Seo⁵

5 *¹Korea Institute of Geoscience and Mineral resources, Daejeon, 34132, South Korea*

6 *²Korea Polar Research Institute, Incheon, 21990, South Korea*

7 *³Department of Atmospheric and Oceanic Sciences, University of California, Los Angeles,*
8 *90095-1565, USA*

9 *⁴School of Earth and Environmental Sciences, Seoul National University, Seoul, 08826, South*
10 *Korea*

11 *⁵Department of Atmospheric Sciences, Pusan National University, Busan, 46241, South*
12 *Korea*

13
14 **Abstract**

15 **The Holocene thermal maximum was characterized by strong summer solar heating**
16 **that substantially increased the summertime temperature relative to pre-industrial**
17 **climate. However, the summer warming was compensated by weaker winter insolation,**
18 **and the annual-mean temperature of the Holocene thermal maximum remains**
19 **ambiguous. Utilizing multi-model mid-Holocene simulations, the authors show that the**
20 **annual-mean Northern Hemisphere temperature is strongly correlated with the degree**
21 **of Arctic amplification and sea ice loss. Specifically, Arctic surface warming is on**
22 **average 3.5 times stronger than that of the northern extratropics (30°N–90°N).**

23 **Additional idealized model experiments show that the summer Arctic sea ice loss**
24 **persists into the winter and increases surface temperatures not only in the Arctic but**
25 **also in mid-latitudes. These results, which are partly evaluated against paleo proxy data,**
26 **suggest that the degree of Arctic amplification is a key for estimating the Northern**
27 **Hemisphere temperature and for solving the Holocene temperature conundrum.**

28

29 **Introduction**

30 Since the end of the last ice age around 12,000 years ago, warming climates have lead to the
31 development of agriculture and the rise of human civilization. This important period is
32 referred to as the Holocene geological epoch (Wanner et al. 2008). During the early-mid
33 Holocene, Northern Hemisphere summer solar insolation was anomalously strong, causing
34 the Holocene thermal maximum (HTM) from around 9,000 years to 5,000 years before
35 present (BP) (Renssen et al. 2009). Pronounced warming at high-latitudes, including
36 Greenland, Western Arctic and Northern Europe, have been associated with the HTM
37 (Kaufman et al. 2004; Larsen et al. 2015; Gajewski et al. 2015; Briner et al. 2016; Braconnot
38 et al. 2012). Proxy data indicate that mid-Holocene Arctic sea ice cover was likely reduced
39 relative to the present (Hanslik et al. 2010; Funder et al. 2011; Müller et al. 2012),

40 The Arctic temperature is closely related to the global-mean temperature in equilibrium
41 climate states (Manabe and Wetherald, 1975; Merlis and Henry 2018), and Arctic warming
42 has been directly linked to warming of the extratropical ocean (Deser et al. 2015; Blackport
43 and Kushner 2018). . Therefore, it is reasonable to assume that the NH was probably warmer
44 during the HTM than during the pre-industrial era, at least in the NH extratropics (30°N–

45 90°N). However, this analogy does not account for the seasonal changes in solar radiation
46 during the HTM: The strong summer solar heating was compensated by the weaker winter
47 insolation and the annual-mean temperatures are difficult to estimate (Renssen et al. 2009;
48 Braconnot et al. 2012; Baker et al. 2017). Additionally, in a climate model simulation, mid-
49 Holocene temperature in northern extratropics (30°N–90°N) was slightly lower than that of
50 the pre-industrial climate (Liu et al. 2014).

51 In this study, we show that the degree of Arctic amplification is closely tied to Northern
52 Hemisphere (NH) annual-mean temperature under mid-Holocene insolation. By utilizing
53 multi-model simulations for the mid-Holocene warm period, we show that the NH
54 temperature anomalies are strongly correlated with Arctic surface temperature and sea ice
55 cover anomalies. Climate models simulating warmer NH climate exhibit much larger Arctic
56 amplification and sea ice loss than others. In these warm models, summer Arctic sea ice loss
57 persists into the winter and increases the mid- and high-latitude temperatures throughout the
58 season. We further show that the northern high-latitude temperatures reconstructed from
59 paleo proxy data agree better with these warm models' estimates. This result may help to
60 resolve the well-known discrepancy between Holocene temperature reconstructions derived
61 from paleo proxy data vs. climate models, which has been coined the 'Holocene temperature
62 conundrum' (Liu et al. 2014).

63

64 **Results**

65 **Arctic and global temperature anomalies in climate models**

66 To assess the climate response to the amplified seasonal insolation forcing during the HTM,
67 we examined the mid-Holocene climate simulated by 13 climate models. Out of 13, 11
68 models were obtained from the Paleoclimate Modelling Intercomparison Project phase 3
69 (PMIP3), while the remaining 2 simulations were conducted by the authors for the purpose of
70 this study (see Methods). The mid-Holocene, which was about 6,000 years BP, belongs to the
71 late period of the HTM and is one of the benchmark periods of PMIP3.

72 Figure 1a shows the globally-averaged mid-Holocene temperature anomalies relative to the
73 pre-industrial climate from the 13 model simulations. A majority of climate models simulate a
74 colder mid-Holocene climate, which is qualitatively consistent with a recent model study (Liu
75 et al. 2014) showing that the global-mean temperature may have increased from the HTM to
76 the present. However, the NH extratropical temperatures averaged over 30°N–90°N show
77 generally warm anomalies: 9 of the 13 models simulate a warmer mid-Holocene than the pre-
78 industrial NH climate (Fig. 1c). For reference, one standard deviation of the annual-mean
79 temperature variations averaged in NH extratropics is less than 0.2 K (estimated from pre-
80 industrial simulations). The three warmest climate models, CNRM-CM5, CESM1-CAM5 and
81 MRI-CGCM3 exhibit more than 0.3 K warming in the mid-Holocene NH. In contrast,
82 NCAR-CCSM4, which was used in the study of Liu et al. (2014), exhibited a 0.25 K cooling
83 in the mid-Holocene. Note that the northern extratropics is the key region where the proxy-
84 based reconstruction (Marcott et al. 2013) shows the largest warm anomalies during the HTM.
85 The composite maps of surface temperature averaged over the four warmest and the four
86 coldest models show that the warmest models simulate an enhanced polar warming,
87 especially in the Arctic (Fig. 1e,f). In the mid-latitudes and sub-Arctic regions (around
88 35°N/S–65°N/S) the signs of temperature anomalies are opposite between the warmest and

89 coldest models. For example, Europe warms in the warmest models (Fig. 1e,f), which is
90 consistent with multiple pollen records (Braconnot et al. 2012; Masson et al. 1999), but no
91 such warming is distinguishable in the coldest models. These regional differences suggest
92 that the relatively warm models simulate stronger climate feedbacks in response to the mid-
93 Holocene insolation forcing.

94 The zonal-mean temperature anomalies exhibit a pattern of warming at high-latitudes and
95 cooling in the tropics (Fig. 1g), and this pattern is generally consistent with the annual-mean
96 insolation anomalies (Supplementary Fig. 1). The warmest models exhibit less tropical
97 cooling, suggesting that the mid-Holocene Arctic amplification may be influenced by tropical
98 temperature. In fact, tropical sea surface temperature (SST), despite its relatively small
99 variations, is known to affect the Arctic amplification through poleward energy transport
100 (Solomon 2006; Lee 2014). Additional idealized climate model experiments (see Methods)
101 indicate that the tropical SST cooling drives moderate cooling in southern extratropics (30°S–
102 50°S) and slight cooling in the adjacent northern extratropics (30°N–45°N) by around 0.1 K
103 (Supplementary Fig. 2). In particular, the western North Pacific cooling in the model is
104 primarily driven by the tropical SST cooling. However, this idealized model experiment also
105 indicates that the tropical SST cooling could slightly increase high-latitude temperature
106 (Supplementary Fig. 2), highlighting the complexity of tropical-extratropical teleconnection
107 in response to tropical heating (Goss et al. 2016).

108 Modeling studies instead suggest the local radiative forcing and the associated feedbacks in
109 the Arctic are more important than teleconnections from the tropics in explaining polar
110 amplification in both the Arctic (Stuecker et al. 2018) and Antarctic (Kim et al. 1998). Recent
111 studies further indicate that the Arctic warming can increase extratropical SSTs (Deser et al.

112 2015), which can in turn accelerate the Arctic warming (Blackport and Kushner 2018).
113 Indeed, Figure 1b shows that the inter-model spread in global-mean temperature is well
114 correlated with that in Arctic temperature with a correlation coefficient of 0.84, which is
115 statistically significant ($p < 0.01$). The correlation between the Arctic and the northern
116 extratropics is even larger, $r = 0.91$ (Fig. 1d). This result implies that the uncertainty in Arctic
117 temperature response to the mid-Holocene insolation forcing explains more than 80% of the
118 variance in the NH temperature responses across the 13 climate models examined here. The
119 multi-model regression line also indicates that the Arctic warming is about 3.5 times stronger
120 than that of the northern extratropics. These robust relationships ($r=0.84$ & $r=0.91$) suggest
121 that the degree of Arctic amplification plays a key role in setting mid-Holocene global
122 temperature, especially in northern extratropics.

123 **Seasonal temperature anomalies in the warmest vs. coldest models**

124 What drives such a large inter-model difference in Arctic temperature responses (Figs 1b, d)?
125 The zonal-mean time-latitude Hovmöller plots of surface temperature show that high-latitude
126 (35°N – 85°N) warming in summer persists into the winter in the warmest models (Fig 2a),
127 whereas the summer warming does not persist in the coldest models (Fig. 2b). These results
128 indicate that the key difference between the warmest and the coldest models is not simply the
129 magnitude of summer heating but also the persistence of summer warming to the winter.

130 It is likely that the seasonally persistent Arctic warming in the warmest models (e.g. CNRM-
131 CM5, CESM1-CAM5) are the outcome of various climate feedbacks associated with Arctic
132 sea ice loss (Pithan and Mauritsen 2014; Goosse et al. 2018). In the warmest models, Arctic
133 sea ice concentration (SIC) in summer-autumn decreases by 30–35% over wide areas of the

134 Arctic relative to the pre-industrial climate (Fig. 2c) and these SIC anomalies persist into
135 winter and early spring over the marginal ice zone (Fig. 2d), indicative of delayed refreezing
136 and reduced ice growth (Markus et al. 2009). This autumn–winter sea ice loss is accompanied
137 by increases in heat transfer from the Arctic Ocean to the atmosphere, primarily through
138 turbulent heat fluxes (Supplementary Fig. 3), further contributing to the Arctic amplification
139 (Screen and Simmonds 2010). The winter SIC anomalies, albeit smaller than those of the
140 summer-autumn, have strong influence on mid-latitude climate (Sun et al. 2015; Nakamura et
141 al. 2016; Blackport and Screen 2019), partly because the reduction of winter SIC is
142 accompanied by reduced ice thickness (Labe et al. 2018). In the coldest models, however, the
143 summer-autumn SIC anomalies are small, generally within 10% (Fig. 2e), and do not persist
144 into the winter (Fig. 2f). In the absence of the Arctic sea ice loss, the northern high-latitudes
145 experience anomalously cold climate (Fig. 2b) because of the weaker winter insolation during
146 the mid-Holocene. Several paleo-proxy records suggest that the eastern Canada and the
147 Atlantic sector of the Arctic experienced substantial reduction of sea ice cover during the
148 HTM (Funder et al., 2011; Müller et al., 2012), lending support to the anomalies simulated by
149 the warmest models. However, it is still unclear whether there was a basin-wide reduction of
150 Arctic SIC (de Vernal et al. 2017).

151 **Rectification of seasonal temperature by Arctic sea ice loss**

152 Because the Arctic sea ice loss is generally confined in latitudes higher than 70°N (Figs 1c,
153 1d), the causality between the sea ice loss and the mid-latitude warming (Fig. 2a) remains
154 elusive. To better quantify the climatic responses to the mid-Holocene Arctic sea ice loss, we
155 performed idealized climate model experiments (see Methods) using CESM1-CAM5, the
156 second warmest model (see Figs. 1a, c). A series of simulations show that the impact of

157 Arctic sea ice loss is not limited to high-latitudes, but extends to warming of the mid-latitudes
158 (Figs. 3a, d). The zonal-mean, latitude–time Hovmöller plot of surface temperature (Fig. 3a)
159 shows that the Arctic sea ice loss can substantially increase the sub-Arctic (60°N–70°N)
160 temperature by around 1.0 K, and that these anomalies extend southwards to around 50°N.
161 Although the Arctic sea ice loss is most pronounced in summer and autumn (Fig. 2c), the
162 associated mid-latitude warming is largest in autumn and winter (Fig. 3a). In contrast, the
163 direct insolation forcing does not contribute to the rectification of seasonal temperature, but
164 amplifies the seasonal cycle; the zonal-mean surface temperature anomalies rapidly increase
165 in summer-autumn but quickly subside in late autumn and become negative in winter (Fig.
166 3b). The seasonal temperature response of CESM1-CAM5 to the total forcing (Fig. 3c: the
167 sum of sea ice loss and insolation forcing) is similar to that of the warmest models (Fig. 2a).
168 These results indicate that the summer Arctic sea ice loss and the related feedback are key to
169 the seasonally persistent mid-high latitude warming of the warmest models shown in Fig. 2a.

170 How does the Arctic sea ice loss increase the mid-latitude temperature? Climate model
171 simulations consistently indicate that the projected Arctic sea ice decline is followed by
172 extratropical ocean warming that enhances the impact of sea ice loss on mid-latitude climate
173 (Deser et al. 2015; Blackport and Kushner 2018). Consistent with previous studies, Fig. 3d
174 shows that Arctic sea ice loss increases the annual-mean SSTs over the North Pacific and the
175 Nordic Seas by more than 0.5 K. This extratropical ocean warming, resulting from the Arctic
176 sea ice loss (Fig. 3d), is generally stronger than that of the direct insolation forcing (Fig. 3e),
177 especially in the sub-Arctic regions. The Arctic sea ice loss also produces a localized ~0.5 K
178 decrease in SSTs in the central North Atlantic, because the Arctic sea ice loss weakens the
179 Atlantic meridional overturning circulation (Sévellec et al. 2017) and shifts the Gulf Stream

180 southward (Deser et al. 2015; Park et al. 2018). However, this localized Atlantic cooling
181 signal is masked under a zonal average (Fig. 3a).

182

183 **Evaluation of climate models against proxy data**

184 Evaluating the climate model simulations against reconstructed proxy data is one of key
185 purposes of PMIP (Masson et al. 1999). While the simulated temperatures are widely
186 different each other (Figs. 1a, c), they are well constrained by the degree of Arctic
187 amplification (Figs 1b, 1d). This strong inter-model correlation could provide a quantitative
188 framework via which to estimate global-scale temperatures from the reconstructed proxy data
189 in the high latitudes. To evaluate the model simulations, we utilized pollen-based dataset
190 assembled by a PMIP working group (Bartlein et al 2011). This dataset, which has $2^\circ \times 2^\circ$
191 spatial resolution, is based on 148 proxy stations in high-latitudes (higher than 60°N), mostly
192 over land (Fig. 4b). To quantitatively compare these proxy data with model simulations, the
193 same grids covered by the proxy data are selected in the climate models (Fig. 4c). Both proxy
194 data (Fig. 4b) and the warm model average (Fig. 4c) exhibit anomalously warm temperatures
195 over Fennoscandia, where proxy data are most abundant. However, regional scale
196 temperature variations are much larger in paleo proxy data than climate model simulations
197 (Braconnot et al. 2012)

198 Annual-mean temperature anomalies averaged over the selected grids are plotted in the
199 abscissa of Fig. 4a. The inter-model temperature difference ranges up to 1.8 K and this is
200 about 30% smaller than that in the Arctic (about 2.5 K as shown in Figs 1b, 1d). Although
201 spatially sparse grids are averaged, these grid-averaged temperatures are well correlated with

202 temperatures averaged in the entire NH extratropics (Fig. 4a). The average proxy-based
203 temperature anomaly is 0.56 K (red dot in Fig. 4a), which is similar to those of the relatively
204 warm climate models such as CESM1-CAM5 and MRI-CGCM3.

205 To further evaluate the models, we utilized another paleo proxy dataset which was compiled
206 from previously published Holocene proxy records in northern high-latitudes (Sundqvist et al.
207 2014). This dataset provides 93 proxy stations for the temperature data. While the number of
208 stations is smaller than that of Bartlein et al. (2011), the temperature records were
209 reconstructed not only from land but also from the Arctic and sub-Arctic Oceans. Consistent
210 with Fig. 4, the average value proxy-based reconstruction of temperature anomalies is similar
211 to those of the warm models (Supplementary Fig. 4). These results indicate that the NH
212 extratropics may have been warmer during the mid-Holocene than in the pre-industrial era,
213 and that the proxy-based estimation of NH annual-mean temperature is generally within the
214 range of model simulations. This suggests that the apparent discrepancy between temperature
215 reconstructions from paleo proxy data and simulated mid-Holocene temperature may be
216 attributable to inter-model variations in the degree of simulated Arctic amplification (Liu et al.
217 2014).

218

219 **Summary**

220 In this study, we present evidence that the annual-mean NH extratropical temperature
221 response to mid-Holocene insolation is strongly constrained by Arctic amplification and sea
222 ice loss. We examined 13 climate models that simulate widely varying temperature responses
223 in the NH extratropics, and found that these temperature anomalies are strongly correlated

224 with the degree of Arctic amplification. The models that exhibited the strongest NH warming
225 and Arctic amplification in the mid-Holocene also simulated pronounced summer warming
226 anomalies that persisted into winter. Idealized climate model perturbation experiments exhibit
227 a similar warming anomaly in response to an isolated loss of Arctic sea ice (see Park et al.,
228 2018), indicating that the response of Arctic sea ice to mid-Holocene insolation is a key
229 discriminator between the models' NH temperature responses. The Arctic sea ice cover
230 during the HTM was likely smaller than the pre-industrial climate, as shown by proxy records
231 (Funder et al., 2011; Müller et al., 2012), which is consistent with a substantial Arctic
232 warming in the mid-Holocene. Unfortunately, the basin-wide reconstruction of mid-Holocene
233 Arctic sea ice cover is not available (de Vernal et al. 2017). As an alternative means of
234 evaluating the model results, we utilized high-latitude (higher than 60°N) pollen-derived
235 temperature reconstructions, and found that the proxy-based temperature anomalies were
236 close to those of the climate models that simulated a warmer NH mid-Holocene. Our results
237 therefore suggest that the relatively warm climate models, simulating rectified temperature
238 increases associated with Arctic sea ice loss, are closer to the proxy-based temperature
239 reconstructions and therefore are more reliable ones for simulating the Holocene climate
240 changes.

241

242 **Methods**

243 **Multi-model simulations (PMIP3)**

244 The mid-Holocene, around 6,000 years BP, is a benchmark period of the Paleoclimate
245 Modeling Intercomparison Project, phase 3 (PMIP3). These simulations are designed to test

246 the climate models' responses to the enhanced seasonal insolation forcing, a key
247 characteristic of the Holocene thermal maximum. The primary difference between the Mid-
248 Holocene and the pre-industrial climate simulations is the orbital forcing. Mid-Holocene CO₂
249 concentration, aerosols, ice sheets, and topography are the same as those of the pre-industrial
250 climate simulation. We evaluated the surface temperature and sea ice concentration fields by
251 examining the differences between PMIP3 mid-Holocene and CMIP5 Pre-Industrial
252 simulations. A list of the PMIP3–CMIP5 models, their Atmosphere and Ocean resolutions,
253 and averaging periods (in years) used for analysis are provided in Table 1.

254 **Two additional mid-Holocene climate model simulations**

255 To supplement the PMIP3 ensemble, we performed simulations using two additional climate
256 models, NCAR CESM1.2.1 (Hurrell et al. 2013) and GFDL CM2.1 (Delworth et al. 2006).
257 By adding two independent climate model simulations to the existing PMIP3, we intend to
258 improve the robustness of our multi-model analyses. We performed the mid-Holocene and
259 pre-industrial climate simulations both for CESM1.2.1 and CM2.1. These model runs were
260 configured and forced in the same way as the existing PMIP3 simulations.

261 **(1) NCAR CESM1.2.1:** The atmospheric component of NCAR CESM1.2.1 is the
262 Community Atmospheric Model version 5 (CAM5) with 30 vertical levels, and the ocean
263 component is the Parallel Ocean Program version 2 (POP2) with 60 vertical levels. The land
264 and sea ice components are the Community Land Model version 4 (CLM4) and the Los
265 Alamos sea ice model version 4 (CICE4), respectively. We integrated this model using a
266 horizontal grid spacing of approximately 1 degree (f09g16). The root-mean-square errors of
267 sea ice extent and volume between CESM1–CAM5 and observations are one of the lowest

268 (Shu et al. 2015) among 49 climate models that have participated in phase 5 of the Coupled
269 Model Intercomparison Project (CMIP5).

270 **(2) GFDL CM2.1:** We also utilized the Coupled Climate Model version 2.1 (CM2.1), which
271 was developed at the Geophysical Fluid Dynamics Lab (GFDL). The atmospheric model
272 (AM2.1) uses a Lagrangian finite-volume dynamical core, with a 2.5° longitude \times 2°
273 latitude and 24 vertical levels. The ocean component is the Modular Ocean Model (MOM)
274 (MOM5.1 in this study), which consists of 50 vertical levels and a constant zonal resolution
275 of 1° , and the meridional resolution varying from 0.33° at the equator to 1° close to the poles.
276 The land and sea ice components are the land model version 2.1 (LM2.1) based on the Land
277 Dynamics Mode and the Sea Ice Simulator (SIS), respectively. We performed simulations of
278 approximately 200 years in duration for both the mid-Holocene and pre-industrial climates.

279

280 **Idealized climate model perturbation experiments**

281 **(1) NCAR CESM1.2.1:** This is the second warmest model in simulating the mid-Holocene
282 climate and exhibits a relatively strong Arctic warming (Fig 1). We utilized this model to test
283 the impact of Arctic sea ice loss on extratropical temperature. To distinguish the climatic
284 responses to sea ice loss and anomalous insolation forcing in the mid-Holocene, we perform
285 three different model simulations:

286 **0 k:** Pre-industrial control simulation (335-year duration)

287 **6 ka:** Mid-Holocene climate simulation (315-year duration)

288 **6 ka with 0 k sea ice:** Mid-Holocene climate with sea ice albedo is increased to 0.91 (316-

289 year duration)

290 For the “**6 ka with 0 k sea ice**” simulation, the mid-Holocene forcing is branched off at year
291 31 of the Pre-industrial run, except the albedo of sea ice is increased globally, and throughout
292 the year, from 0.73 to 0.91 to reflect more sunlight, while the snow albedo over sea ice is not
293 changed. Recent studies (Blackport and Kushner 2017; Park et al. 2018) also used this
294 method (changing sea ice albedo) to distinguish the impact of Arctic sea loss from the direct
295 effect of mid-Holocene insolation anomalies. The increased ice albedo simulation maintains
296 the Arctic sea ice cover by reflecting anomalously strong 6 ka summer insolation, keeping
297 SIC anomalies within 5% of the preindustrial simulation in summer and autumn (Park et al.
298 2018). A more detailed description of these idealized model experiments is given by Park et
299 al. (2018).

300 The contributions of Arctic sea ice loss and direct insolation anomalies to mid-Holocene
301 climate, relative to the preindustrial, can be separated as follows:

302 The contribution of **Arctic sea ice loss: (6 ka) – (6 ka with 0 k sea ice)**

303 The contribution of **insolation forcing: (6 ka with 0 k sea ice) – (0 k)**

304 In each simulation, we perform analysis using the last 250 years.

305

306 **(2) GFDL CM2.1:** This model’s global and northern extratropical temperature responses to
307 mid-Holocene insolation forcing are close to the multi-model averages, neither being too
308 warm nor cold (Figs 1a, 1c). Similar to the multi-model averages, this model also exhibits a
309 pattern of warming in the high-latitudes and cooling in the tropics (Supplementary Fig. 2). To

310 isolate the impact of this tropical SST cooling on global temperature, especially on the Arctic
311 amplification, we performed an idealized mid-Holocene climate experiment, in which the
312 tropical (30°S–30°N) SSTs were continuously restored to those of the pre-industrial climate.

313 These simulations are summarized as follows:

314 **6 ka:** Mid-Holocene climate simulation (208-year duration)

315 **6 ka with 0 k tropical SSTs:** Mid-Holocene climate with tropical SSTs are restored to those
316 of 0 k with a restoring timescale of 5 days (165-year duration)

317 The contributions of the tropical SST cooling to mid-Holocene climate can be separated as
318 the difference between these two simulations:

319 The contribution of **tropical SST cooling: (6 ka) – (6 ka with 0 k tropical SSTs)**

320 In each simulation, we perform analysis using the last 150 years. These simulation results are
321 presented in Supplementary Fig. 2.

322

323 **Data availability**

324 Monthly climate model outputs, for both the NCAR CESM1.2.1 and GFDL CM2.1
325 simulations conducted for the purpose of this study, are available on *Earth* Linux cluster
326 sever at Korea Institute of Geoscience and Mineral Resources (KIGAM). Several daily
327 output variables are also available. These monthly and daily data are available from the
328 corresponding author upon reasonable request. PMIP3 mid-Holocene and CMIP5 pre-

329 industrial control simulation outputs are available to download at [https://esgf-
331 node.llnl.gov/projects/cmip5/.](https://esgf-
330 node.llnl.gov/projects/cmip5/)

332 **References**

- 333 1. Wanner, H. et al. Mid- to late Holocene climate change: An overview. *Quat. Sci. Rev.*
334 **27**, 1791–1828 (2008).
- 335 2. Renssen, H. et al. The spatial and temporal complexity of the Holocene thermal
336 maximum. *Nature Geosci.* **2**, 411–414 (2009).
- 337 3. Kaufman, D. S. et al. Holocene thermal maximum in the western Arctic (0–180°W).
338 *Quat. Sci. Rev.* **23**, 529–560 (2004).
- 339 4. Larsen, N. K. et al. The response of the southern Greenland ice sheet to the Holocene
340 thermal maximum. *Geology.* **43**, 291–294 (2015).
- 341 5. Gajewski K. Quantitative reconstruction of Holocene temperatures across the
342 Canadian Arctic and Greenland. *Global and Planetary Change.* **128**, 14–23 (2015).
- 343 6. Briner, J. P. et al. Holocene climate change in Arctic Canada and Greenland. *Quat.*
344 *Sci. Rev.* **147**, 340–364 (2016).
- 345 7. Braconnot, P. et al. Evaluation of climate models using palaeoclimatic data. *Nature*
346 *Clim. Change.* **2**, 417–424 (2012).
- 347 8. Hanslik, D. et al. Quaternary Arctic Ocean sea ice variations and radiocarbon
348 reservoir age corrections. *Quat. Sci. Rev.* **29**, 3430–3441 (2010).
- 349 9. Funder, S. et al. A 10,000-year record of Arctic Ocean sea-ice variability—view from
350 the beach. *Science.* **333**, 747–750 (2011).
- 351 10. Müller, J. et al. Holocene cooling culminates in sea ice oscillations in Fram Strait.
352 *Quat. Sci. Rev.* **47**, 1–14 (2012).

- 353 11. Manabe, S. & Wetherald, R. T. 1975: The effect of doubling the CO₂ concentration
354 on the climate of a general circulation model. *J. Atmos. Sci.* **32**, 3–15 (1975).
- 355 12. Merlis, T. M. & Henry, M. Simple estimates of polar amplification in moist diffusive
356 energy balance models. *J Climate*. **31**, 5811–5824 (2018).
- 357 13. Deser, C., Tomas, R. A. & Sun, L. The role of ocean-atmosphere coupling in the
358 zonal-mean atmospheric response to Arctic sea ice loss. *J. Climate*. **28**, 2168–2186
359 (2015).
- 360 14. Blackport, R. & Kushner, P. J. The Role of Extratropical Ocean Warming in the
361 Coupled Climate Response to Arctic Sea Ice Loss. *J Climate*. **31**, 9193–9206 (2018).
- 362 15. Baker, J. L., Lachniet, M. S., Chervyatsova, O., Asmerom, Y. & Polyak, V. Holocene
363 warming in western continental Eurasia driven by glacial retreat and greenhouse
364 forcing. *Nature Geosci.* **10**, 430–436 (2017).
- 365 16. Liu, Z. et al. The Holocene temperature conundrum. *Proc. Natl Acad. Sci. USA*. **111**,
366 E3501–E3505 (2014).
- 367 17. Marcott, S. A., Shakun, J. D., Clark, P. U. & Mix, A. C. A reconstruction of regional
368 and global temperature for the past 11,300 years. *Science*. **339**, 1198–1201 (2013).
- 369 18. Masson, V., Cheddadi, R., Braconnot, P., Jousaume, S., Texier, D. & PMIP
370 participants. Mid-Holocene climate in Europe: what can we infer from PMIP model-
371 data comparisons? *Clim Dyn.* **15**, 163–182 (1999).
- 372 19. Solomon, A. Impact of latent heat release on polar climate. *Geophys. Res. Lett.* **33**,
373 L07716 (2006).
- 374 20. Lee, S. A theory for polar amplification from a general circulation perspective. *Asia-
375 Pac. J. Atmos. Sci.* **50**, 31–43 (2014).
- 376 21. Goss, M., S. B. Feldstein. & S. Lee. Stationary wave interference, and its relation to
377 tropical convection and Arctic warming. *J. Climate*. **29**, 1369–1389 (2016).
- 378 22. Stuecker, M. F., C. M. Bitz, K. C. Armour, C. Proistosescu, S. M. Kang, S.-P. Xie, D.

- 379 Kim, S. McGregor, W. Zhang, S. Zhao, W. Cai, Y. Dong. & F.-F. Jin. Polar
380 amplification dominated by local forcing and feedbacks. *Nature Climate Change*. **8**,
381 1076–1081 (2018).
- 382 23. Kim, S.-J., Crowley, T. J. & Stossel, A. Local orbital forcing of Antarctic climate
383 change during the last interglacial. *Science*. **280**, 728–730 (1998).
- 384 24. Pithan, F. & Mauritsen, T. Arctic amplification dominated by temperature feedbacks
385 in contemporary climate models. *Nature Geosci.* **7**, 181–184 (2014).
- 386 25. Goosse, H. et al. Quantifying climate feedbacks in polar regions. *Nature Comms*, **9**,
387 1919 (2018).
- 388 26. Markus, T., Stroeve, J. C. & Miller, J. Recent changes in Arctic sea ice melt onset,
389 freezeup and melt season length. *J. Geophys. Res.* **114**, C12024 (2009).
- 390 27. Screen, J.A. & Simmonds, I. Increasing fall-winter energy loss from the Arctic Ocean
391 and its role in Arctic temperature amplification. *Geophys. Res. Lett.* **37**, L16797
392 (2010).
- 393 28. Sun, L., Deser, C. & Tomas, R. A. Mechanisms of stratospheric and tropospheric
394 circulation response to projected Arctic sea ice loss. *J. Climate*. **28**, 7824–7845
395 (2015).
- 396 29. Nakamura, T. et al. The stratospheric pathway for Arctic impacts on midlatitude
397 climate, *Geophys. Res. Lett.* **43**, 3494–3501 (2016).
- 398 30. Blackport, R. & Screen, J. A. Influence of Arctic sea-ice loss in autumn compared to
399 that in winter on the atmospheric circulation. *Geophys. Res. Lett.*
400 <https://doi.org/10.1029/2018GL081469> (2019).
- 401 31. Labe, Z.M., Peings, Y. & Magnusdottir G. Contributions of ice thickness to the
402 atmospheric response from projected Arctic sea ice loss. *Geophys. Res. Lett.*,
403 DOI:10.1029/2018GL078158 (2018).
- 404 32. de Vernal, A., Gersonde, R., Goosse, H., Seidenkrantz, M.-S. & Wolff, E. W. Sea ice

- 405 in the paleoclimate system: the challenge of reconstructing sea ice from proxies—an
406 introduction. *Quat. Sci. Rev.* **79**, 1–8 (2013).
- 407 33. Sévellec, F., Fedorov, A. V. & Liu, W. Arctic sea-ice decline weakens the Atlantic
408 Meridional Overturning Circulation. *Nature Clim. Change.* **7**, 604–610 (2017).
- 409 34. Park, H.-S., Kim, S.-J., Stewart, A. L., Seo, K.-H., Kim, S.-Y. & Son, S.-W. The
410 impact of Arctic sea ice loss on mid-Holocene climate. *Nature Comms*, **9**, 4571
411 (2018).
- 412 35. Bartlein, P. J. et al. Pollen-based continental climate reconstructions at 6 and 21 ka: A
413 global synthesis. *Clim. Dynam.* **37**, 775–802 (2011).
- 414 36. Sundqvist, H. S. et al. Arctic Holocene proxy climate database – new approaches to
415 assessing geochronological accuracy and encoding climate variables. *Climate of the*
416 *Past*, **10**, 1605–1631 (2014).
- 417 37. Hurrell, J. W. et al. The Community Earth System Model: A framework for
418 collaborative research. *Bull. Amer. Meteor. Soc.*, **94**, 1339–1360 (2013).
- 419 38. Delworth, T. L., Broccoli, A. J., Rosati, A., Stouffer, R. J., Balaji, V., Beesley, J. A., et
420 al. GFDL's CM2 global coupled climate models. Part I: Formulation and simulation
421 characteristics. *J. Climate.* **19**, 643–674 (2006).
- 422 39. Shu, Q., Song, Z. & Qiao, F. Assessment of sea ice simulations in the CMIP5 models,
423 *The Cryosphere*, **9**, 399–409 (2015).
- 424 40. Blackport, R. & Kushner, P. J. Isolating the Atmospheric Circulation Response to
425 Arctic Sea Ice Loss in the Coupled Climate System. *J. Climate.* **30**, 2163–2185
426 (2017).

427

428

429 **Acknowledgement:** H.-S. Park was supported by the Basic Research Project (GP2017-013)

430 of the Korea Institute of Geoscience and Mineral Resource (KIGAM), Ministry of Science,
431 ICT, and Future Planning. S.-J. Kim was supported by KOPRI project No. PE18010. S.-W.
432 Son was supported by the National Research Foundation of Korea (NRF) grant NRF-
433 2018R1A5A1024958. A. L. Stewart was supported by National Science Foundation under
434 Grants ANT-1543388 and OCE-1751386. The authors thank Ms. S.-Y. Kim and Mr. J.-S.
435 Kang for collecting and providing the PMIP3 data.

436

437 **Author Contributions:** H.-S. Park initiated the project and carried out the analysis under the
438 guidance of S.-J. Kim. The manuscript was initially written by H.-S. Park and was edited by
439 A. L. Stewart. All authors contributed to the interpretations of the results and the discussion
440 of the manuscript.

441

442 **Competing interests:** The authors declare no competing interests.

443

444 **Corresponding author:** Correspondence to Hyo-Seok Park (hspark1@gmail.com)

445

446

447 **Figure Legends**

448 **Figure 1: Global and Arctic surface temperature simulated by 13 climate models: (a, c)**

449 The mid-Holocene surface temperature anomalies (differences between 6 ka and 0 k) of 13
450 different climate models, averaged **(a)** globally (90°S–90°N) and in **(c)** NH extratropics
451 (30°N–90°N). **(b, d)** The multi-model correlations of surface temperature anomalies between
452 **(b)** the Arctic (70°N–90°N) and the global average as well as between **(d)** the Arctic and the
453 NH extratropics. **(e, f)** Composite maps of the annual-mean surface temperature anomalies,
454 averaged for the **(e)** 4 warmest and the **(f)** 4 coldest models. **(g)** The zonal-mean surface
455 temperature anomalies as a function of latitude, averaged for the 4 warmest (red line) and the
456 4 coldest (blue line) models.

457

458 **Figure 2: Surface temperature and Arctic sea ice responses: (a, b)** Zonally averaged,

459 latitude–time Hovmöller plots of anomalous surface temperature (K) in the **(a)** 4 warmest
460 models and **(b)** 4 coldest models. The abscissa is time (months) and the ordinate is latitude.
461 Arctic sea ice concentration (%) anomalous in the **(c, d)** 4 warmest models and **(e, f)** 4
462 coldest models, averaged in **(c, e)** July–November and **(d, f)** December–April.

463

464 **Figure 3: Disentangling the impacts of Arctic sea ice loss and insolation forcing: Surface**

465 temperature responses to mid-Holocene **(a, d)** Arctic sea ice loss, **(b, e)** insolation forcing and
466 **(c, f)** total forcing (sum of sea ice loss and insolation). **(a, b, c)** Zonally averaged, latitude–
467 time Hovmöller plots of anomalous surface temperature and **(d, e, f)** the annual-mean SST
468 anomalies. In **(a, b, c)**, the abscissa is time (months) and the ordinate is latitude.

469

470 **Figure 4: Validating the climate models against paleo proxy data: (a)** Correlation of

471 surface temperature anomalies between the sub-Arctic (60°N–77°N) averaged over the grids
472 where paleo proxy data exist (abscissa) and the entire NH extratropics (30°N–90°N)
473 (ordinate). The green dots are from the 13 climate models and the red dot is from the paleo

474 proxy data. Sub-Arctic surface temperature anomalies **(b)** reconstructed from the paleo proxy
475 data and **(c)** simulated by 4 warmest climate models over the grids where the paleo proxy
476 data exist.

477

478

479

480

481

482

483

484

485

486

487

488

489

490

491

492

493

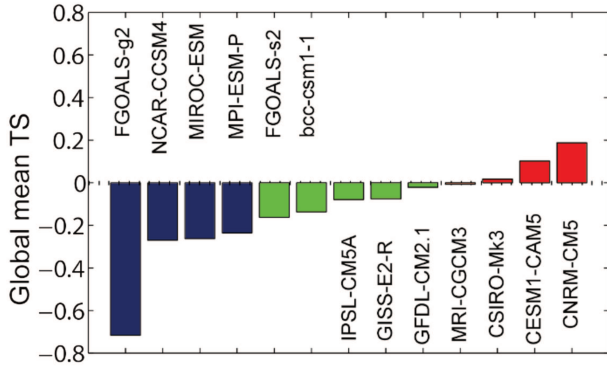
494

495 **Table 1.** Summary of the PMIP3 simulations and two additional climate model simulations
 496 conducted for the purpose of this study. The fourth and fifth columns indicate the averaging
 497 periods (years) for the pre-industrial (0 ka) and the mid-Holocene (6 ka) simulations,
 498 respectively.

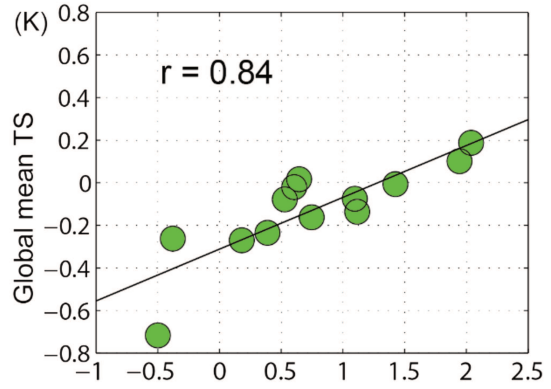
PMIP3 Models	Atmos. resolutions (lat x lon lev)	Ocean resolutions (lat x lon lev)	0 ka (years)	6 ka (years)
BCC-CSM-1	T42 L26	360×232 L40	500	100
NCAR-CCSM4	0.9°×1.25° L26	320×384 L60	1,050	300
CNRM-CM5	T127 L31	362×292 L42	850	200
CSIRO-Mk3-6-0	T63 L18	192×192 L31	500	100
FGOALS-g2	2.81°×2.81° L26	360×196 L30	700	685
FGOALS-s2	1.67°×2.81° L26	360×196 L30	501	100
GISS-E2-R	2.0°×2.5° L40	288×180 L32	1,200	100
IPSL-CM5A-LR	1.875°×3.75° L39	182×149 L31	1,000	500
MIROC-ESM	2.8°×2.8° L80	256×192 L44	630	100
MPI-ESM-P	T63 L47	256×220 L40	1,150	100
MRI-CGCM3	TL159 L48	364×368 L51	500	100
Additional Models	Atmos. Resolutions	Ocean resolutions	0 ka (years)	6 ka (years)
CESM1-CAM5	0.9°×1.25° L26	gx1v6 L60	250	250
GFDL-CM2.1	2.0°×2.5° L24	360×384 L50	150	150

499

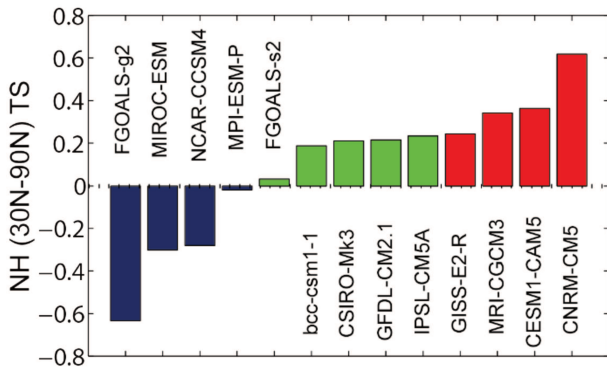
(a) Global mean TS anomalies



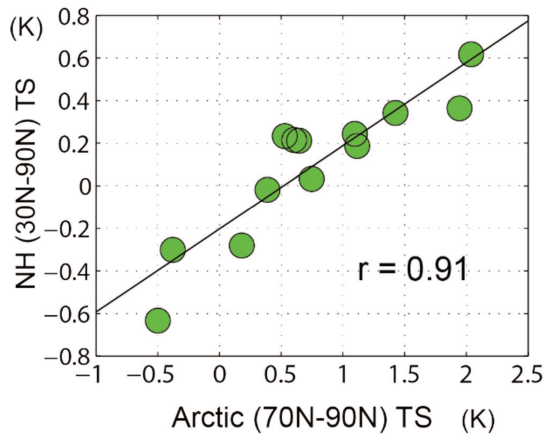
(b) Correlation: Arctic vs. Global



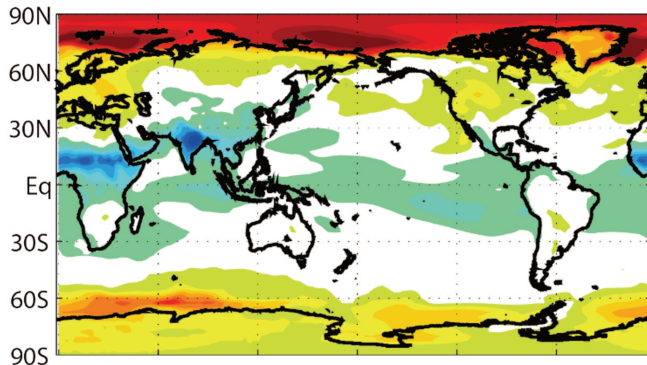
(c) NH (30N-90N average) TS anomalies



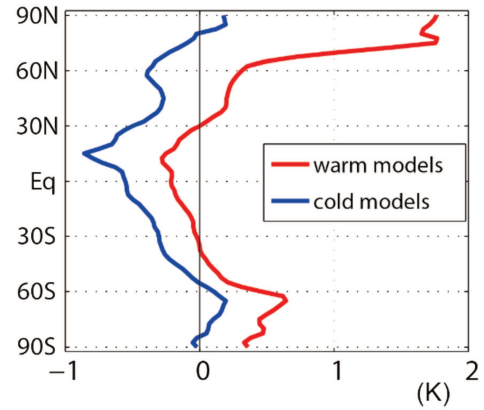
(d) Correlation: Arctic vs. NH



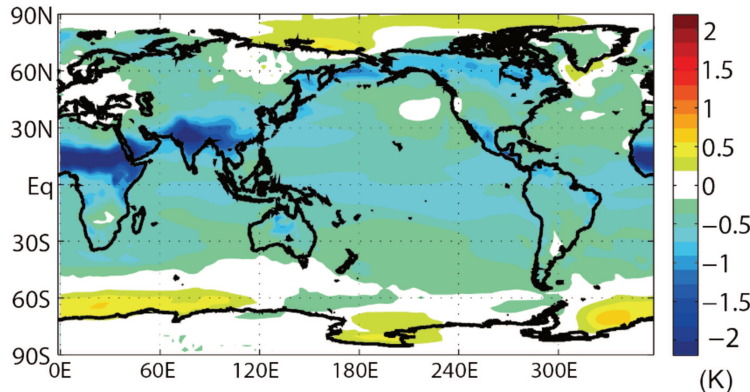
(e) 4 Warmest model TS anomalies



(g) Zonal-mean TS anomalies



(f) 4 Coldest model TS anomalies



501 **Figure 1: Global and Arctic surface temperature simulated by 13 climate models: (a, c)**
502 The mid-Holocene surface temperature (TS) anomalies (differences between 6 ka and 0 k) of
503 13 different climate models, averaged **(a)** globally (90°S–90°N) and **(c)** in the NH
504 extratropics (30°N–90°N). **(b, d)** The multi-model correlations of surface temperature
505 anomalies **(b)** between the Arctic (70°N–90°N) and the global average as well as **(d)** between
506 the Arctic and the NH extratropics. **(e, f)** Composite maps of the annual-mean surface
507 temperature anomalies, averaged for the **(e)** 4 warmest and the **(f)** 4 coldest models. **(g)** The
508 zonal-mean surface temperature anomalies as a function of latitude, averaged for the 4
509 warmest (red line) and the 4 coldest (blue line) models.

510

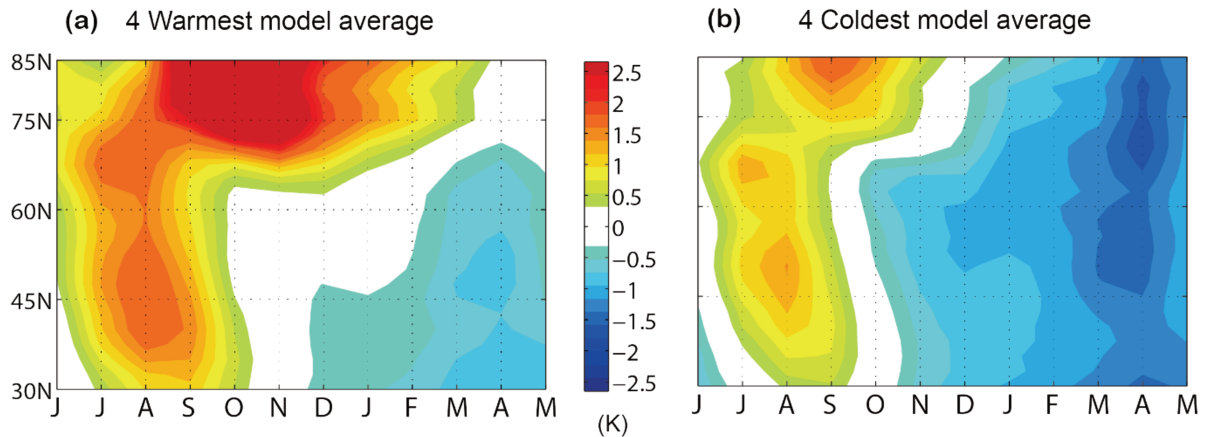
511

512

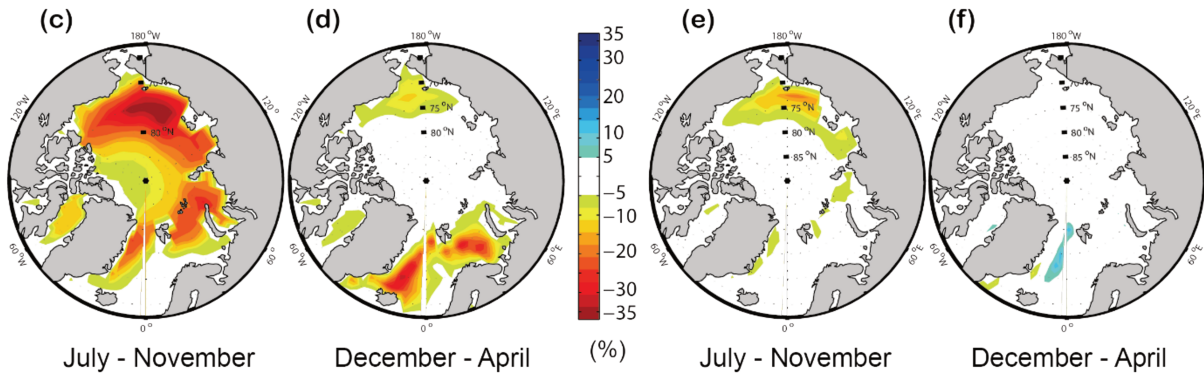
513

514

Hovmoller plot of surface temperature



sea ice concentration



515

July - November

December - April

(%)

July - November

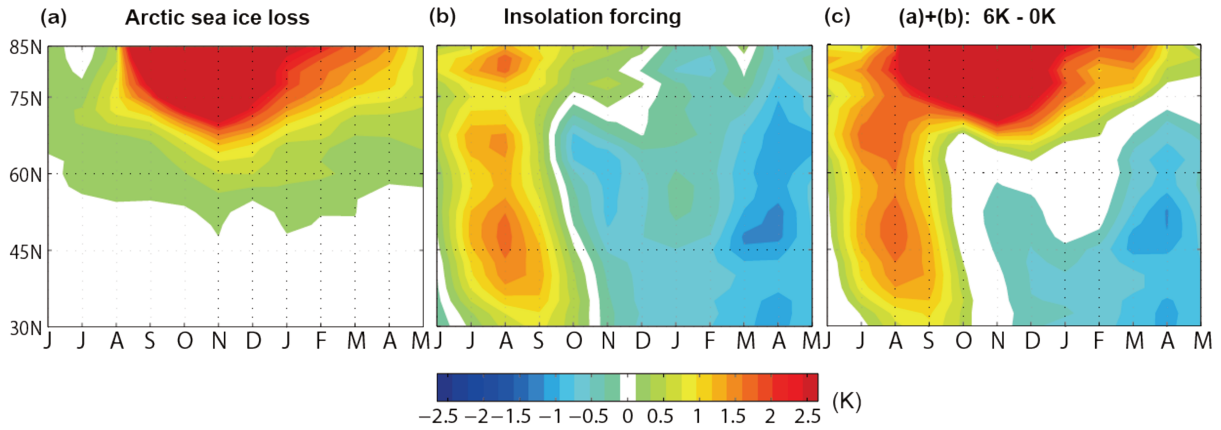
December - April

516

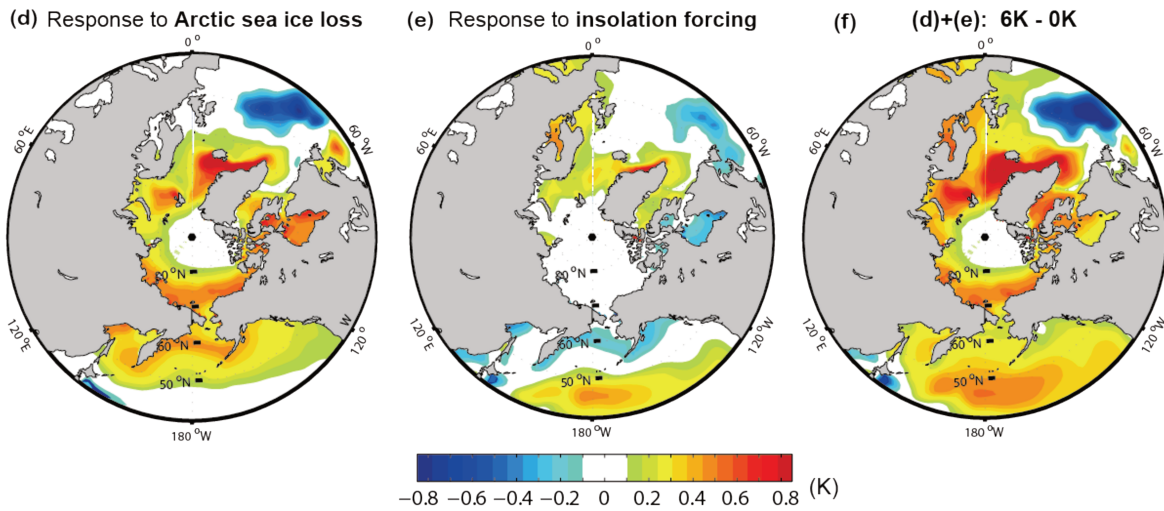
517 **Figure 2: Surface temperature and Arctic sea ice responses:** (a, b) Zonally averaged,
 518 latitude–time Hovmöller plots of anomalous surface temperature in (a) the 4 warmest models
 519 and (b) the 4 coldest models. The abscissa is time (months) and the ordinate is latitude. Arctic
 520 sea ice concentration (%) anomalies in the (c, d) 4 warmest models and (e, f) 4 coldest
 521 models, averaged in (c, e) July–November and (d, f) December–April.

522

Hovmoller plot of surface temperature



Sea surface temperatures



523

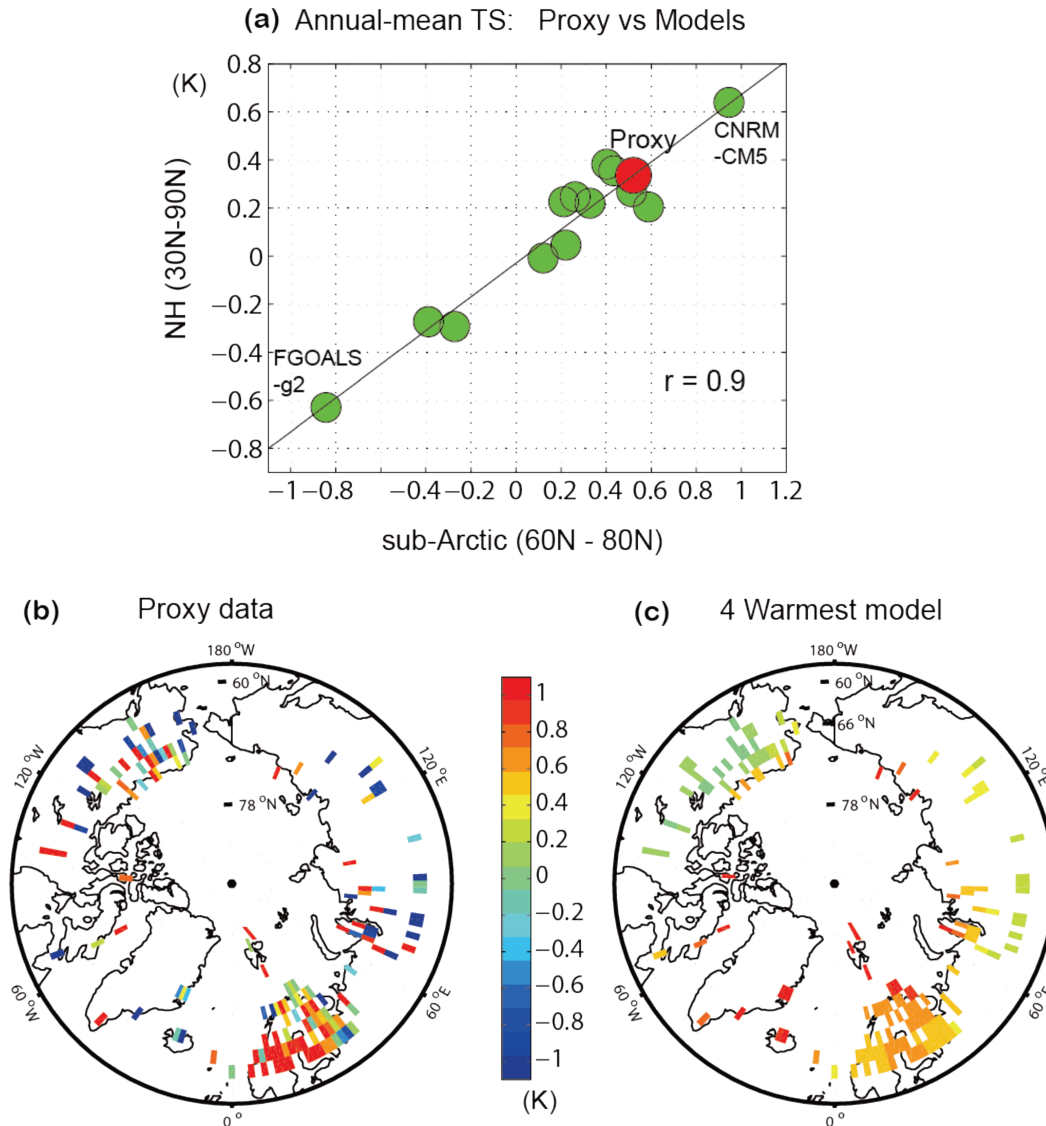
524

525 **Figure 3: Disentangling the impacts of Arctic sea ice loss and insolation forcing:** Surface
 526 temperature responses to mid-Holocene **(a, d)** Arctic sea ice loss, **(b, e)** insolation forcing and
 527 **(c, f)** total forcing (sum of sea ice loss and insolation). **(a, b, c)** Zonally averaged, latitude–
 528 time Hovmöller plots of anomalous surface temperature and **(d, e, f)** the annual-mean SST
 529 anomalies. In **(a, b, c)**, the abscissa is time (months) and the ordinate is latitude.

530

531

532



533

534

535 **Figure 4: Evaluating the climate models against paleo proxy data:** (a) Correlation of
 536 surface temperature (TS) anomalies between the sub-Arctic (60°N–77°N) averaged over the
 537 grids where paleo proxy data exist (abscissa) and the entire NH extratropics (30°N–90°N)
 538 (ordinate). The green dots are from the 13 climate model simulations examined in this study,
 539 and the red dot is from the paleo proxy data. Sub-Arctic surface temperature anomalies (b)
 540 reconstructed from the paleo proxy data and (c) simulated by the 4 warmest climate models
 541 over the grid points at which the paleo proxy estimates are available.

542